Nano Energy 46 (2018) 436–446

Contents lists available at ScienceDirect

Nano Energy

journal homepage: www.elsevier.com/locate/nanoen

Full paper

^{25}Mg NMR and computational modeling studies of the solvation structures and molecular dynamics in magnesium based liquid electrolytes

Jian Zhi Hu[a,*,1], Nav Nidhi Rajput[b,1], Chuan Wan[a,d,2], Yuyan Shao[a,2], Xuchu Deng[a,c], Nicholas R. Jaegers[a], Mary Hu[a], Yingwen Chen[a], Yongwoo Shin[b], Joshua Monk[f], Zhong Chen[c], Zhaohai Qin[d], Karl Todd Mueller[a,*], Jun Liu[a,*], Kristin A. Persson[b,e,*]

[a] The Joint Center for Energy Storage Research (JCESR), Pacific Northwest National Laboratory, Richland, WA 99352, USA
[b] Lawrence Berkeley National Laboratory, Berkeley, CA 94720, USA
[c] Department of Electronic Science, Xiamen University, Xiamen 361005, China
[d] College of Science, China Agricultural University, Beijing 100193, China
[e] Department of Materials Science & Engineering, University of California, Berkeley, CA 94720-1760, USA
[f] AMA Inc., Thermal Protection Materials Branch, NASA Ames Research Center, Moffett Field, CA 94035, USA

ARTICLE INFO

Keywords:
Magnesium battery
$Mg(BH_4)_2$
$Mg(TFSI)_2$
Solvation structures
^{25}Mg NMR
Classical molecular dynamics calculations

ABSTRACT

There is increasing evidence that the solvation structure of the active components in a liquid electrolyte solution strongly impacts the performance in electrochemical applications. In this work, the nanoscale solvation structures and dynamics of $Mg(BH_4)_2$ and $Mg(TFSI)_2$ dissolved in diglyme (DGM) at various concentrations and ratios of $Mg(BH_4)_2$/$Mg(TFSI)_2$ were investigated using a combination of natural abundance ^{25}Mg NMR, quantum chemistry calculations of ^{25}Mg NMR chemical shifts, classical molecular dynamics (MD) calculations, and electrochemical performance tests. By mixing two competing Mg salts, we were able to reduce the strong covalent interactions between Mg^{2+} and BH_4^- anions. A small increase is observed in the coordination number of Mg-TFSI and a significant increase in the interaction of Mg^{2+} ions with glymes. Through a combination of NMR, DFT and MD simulations, various stable species around 1 nm in size were detected in the mixed salt solution, which play key roles in the enhanced electrochemical performance of the mixed electrolyte. It is established that for the neat $Mg(TFSI)_2$ in DGM electrolyte at dilute concentrations the $TFSI^-$ is fully dissociated from Mg^{2+}. At higher concentrations, Mg^{2+} and $TFSI^-$ are only partially dissociated as contact ion pairs are formed. In contrast, at 0.01 M $Mg(BH_4)_2$ (saturated concentration) in DGM, the first solvation shell of a Mg^{2+} ion contains two BH_4^- anions and one DGM molecule, while the second solvation shell consists of five to six DGM molecules. An exchange mechanism between the solvation structures in the combined electrolyte containing both $Mg(BH_4)_2$ and $Mg(TFSI)_2$ in DGM was found to result in the observation of a single ^{25}Mg NMR peak. This exchange is responsible for an increase in uncoordinated anions, as well as improved stability and ionic conductivity as compared to single anion solution. Solvent molecule rearrangement and direct Mg-ion exchange between the basic solvation structures are hypothesized as likely reasons for the exchange. We elucidate that the solvent rearrangement is energetically much more favorable than direct Mg-ion hopping and is thus suggested as the dominant exchange mechanism.

1. Introduction

Recently, there has been an increased interest in the solvation structure of electrolytes as many of their important properties such as conductivity, viscosity, and even stability can be influenced by the local intermolecular interactions in the liquid [1–7]. The solvation structure of electrolytes refers to the detailed molecular interaction between molecular or ionic solutes and other species in solution, e.g. solvent molecules, such that the solute is surrounded by concentric shells of electrolyte molecules to form solvation complexes [8]. For energy applications, so-called 'designer' electrolytes, which are rationally developed to target specific solvation structures, have recently been shown to increase the electrolyte stability [9–13], which is particularly important for nascent energy storage technologies such as Li-S, Li-O, and

* Corresponding authors.
E-mail addresses: Jianzhi.Hu@pnnl.gov (J.Z. Hu), Karl.Mueller@pnnl.gov (K.T. Mueller), Jun.Liu@pnnl.gov (J. Liu), kapersson@lbl.gov (K.A. Persson).
[1] These authors have equal contribution to this work.
[2] These authors have equal contribution to this work, but less than that of Jian Zhi Hu and Nav Nidhi Rajput.

https://doi.org/10.1016/j.nanoen.2018.01.051
Received 25 October 2017; Received in revised form 16 January 2018; Accepted 30 January 2018
Available online 02 February 2018
2211-2855/

multivalent intercalation [2,14–17]. In this work, we focus on elucidating the solvation structure in an organic liquid containing two different competing anions, which enables tuning of the solvation structure as a function of the separate salt concentrations. The common salt cation is chosen as Mg, which is motivated by the need for novel multivalent electrolytes with increased stability for electrochemical energy storage applications [1,3,4,18–28]. In particular, a rechargeable Mg metal battery is an attractive future alternative to Li-ion as it could potentially triple the volumetric energy density (3833 mA h/cc) as compared to the Li counterpart graphite (~800 mA h/cc) [29]. On the other hand, despite the potential advantages, several obstacles need to be addressed, including the need for an electrolyte with a wide electrochemical window which also enables reversible plating/stripping of Mg [30]. The latter requirement is challenging as Mg metal forms an ionically blocking surface layer, i.e., the solid electrolyte interface (SEI), when exposed to oxygen, which inhibits Mg deposition [31]. Hence, the discovery of novel electrolytes in which no SEI or a weakened passivation layer is formed on the Mg metal surface is crucial for realizing highly reversible Mg metal deposition/dissolution [2,32–34]. Electrolytes based on halo, organo, and organo-halo salts in ether solvents were found capable of reversible Mg deposition/dissolution by providing a passivation-free interface [35,36]. However, Grignard solutions are limited by their insufficient anodic stability (< 2 V) and poor conductivity. Their nucleophilic and corrosive nature also makes them incompatible for use with high voltage electrophilic cathodes materials (such as sulfur and oxygen) and aluminum current collectors [35]. Non-nucleophilic electrolytes such as a HMDSMgCl/$AlCl_3$ (THF) solution offer a wider electrochemical stability window (~ 3.3 V) and compatibility with sulfur cathodes, but suffer from capacity fading after the first cycle possibly due to the dissolution of polysulfide species and corrosion of current collectors due to the presence of chloride ions [37]. Simple and non-corrosive inorganic Mg salts such as $Mg(TFSI)_2$ and $Mg(BH_4)_2$ have gained much popularity over the last few years. Mohtadi *et al.* successfully pioneered the use of magnesium borohydride, $Mg(BH)_4$, taking advantage of its high thermodynamic and reductive stability [38]. However, the major drawbacks of $Mg(BH_4)_2$ are the low anodic stability (1.7 V vs. Mg on Pt) and low solubility. On the other hand, magnesium(II) bis(trifluoromethane sulfonyl) imide ($Mg[N(SO_2CF_3)_2]_2$), commonly known as $Mg(TFSI)_2$), has also been reported as a highly competent electrolyte candidate due to its high resistivity towards oxidation, high conductivity, and compatibility with most cathode materials [36]. Unfortunately, it is limited by its high overpotential and low coulombic efficiency for deposition and dissolution [39,40]. Previous reports have shown that the solvent or ligand dramatically influences the electrochemical properties of the electrolytes [10,40,41]. For example, Shao *et. al.* demonstrated that the coulombic efficiency of $Mg(BH_4)_2$ can be significantly enhanced by increasing the ligand strength, i. e. O donor denticity of the ethereal solvents [42]. However, little is known about the detailed changes of the solvation structures and dynamics in Mg electrolyte systems as a function of concentration – particularly when more than one salt is involved. In an effort to design halogen free (non-corrosive) and simple ionic electrolytes, we considered that combining two competing salts, $Mg(BH_4)_2$ and $Mg(TFSI)_2$, would allow for exploration of the tunability of the solvation structure to access the different properties of the salts; BH_4 for its excellent metal plating performance and TFSI for its exceptional redox stability and solubility. Recent studies have shown that the high overpotential for Mg plating/stripping and poor faradaic cycling efficiency of $Mg(TFSI)_2$ electrolyte may be resolved by the addition of chloride ions [43–45]. However, chloride-containing magnesium electrolytes are corrosive towards non-noble metals [7]. A potential solution is to combine $Mg(TFSI)_2$ with $Mg(BH_4)_2$ to access a combination of stability and solubility.

In this work, we adopted a multi-modal approach by combining theory and experiments at multiple lengths and time scales to elucidate the solvation structures as well as electrochemical performance of Mg $(BH_4)_2$ and $Mg(TFSI)_2$ dissolved in diglyme (DGM) at various concentrations and ratios of $Mg(BH_4)_2/Mg(TFSI)_2$ using a combination of natural abundance ^{25}Mg NMR, quantum chemistry calculations of ^{25}Mg NMR chemical shifts, classical molecular dynamics simulations, cyclic voltammetry, and coulombic efficiency measurements. We reveal the exchange mechanism between the basic nanometer sized solvation structures in the mixed electrolyte containing both $Mg(BH_4)_2$ and $Mg(TFSI)_2$ in DGM as the primary factor contributing to the enhanced electrochemical performance achieved with this system. The objective of our research is thus to understand the fundamental solvation structure and exchange mechanisms in these electrolytes such that new design rules for multivalent electrolytes exploiting competing anion interactions lead to enhanced electrochemical performance via unique structural and dynamical properties.

2. Methodology

2.1. Experimental details

2.1.1. Materials and sample preparations

Magnesium borohydride ($Mg(BH_4)_2$, 95%) was purchased from Sigma–Aldrich. Diglyme (DGM) was obtained from Novolyte Technologies, Inc. (Cleveland, US). $Mg(TFSI)_2$ was obtained from Solvionic SA France. All sample preparations were performed in a MBraun Labmaster Ar-filled glove box (Stratham, NH) with water and O_2 contents less than 1 ppm. A variety of samples containing a mix of $Mg(BH_4)_2$ and $Mg(TFSI)_2$, were prepared by dissolving a constant concentration of 0.01 M $Mg(BH_4)_2$ and variable concentrations of $Mg(TFSI)_2$, i.e., from 0 to 0.04 M, in the DGM solvent. Pure 0.01 M $Mg(BH_4)_2$ in DGM and pure 0.005–0.4 M $Mg(TFSI)_2$ in DGM are included to establish cases for the two extremes. Mixtures of $Mg(BH_4)_2$ and $Mg(TFSI)_2$ in DGM with both high $Mg(BH_4)_2$ and high $Mg(TFSI)_2$ concentrations of equal or greater than 0.1 M are also investigated. Detailed sample information is summarized in Table 1, Fig. S1 and Fig. S2 of Supporting Information.

2.1.2. NMR measurements

All ^{25}Mg NMR experiments were performed on a Varian-Agilent 900 MHz NMR spectrometer equipped with a homemade 15 mm outer diameter large-sample-volume probe [46–48], where the advantages of the significantly increased sensitivity from the use of the combined high magnetic field and larger-sample-volume allow for ^{25}Mg NMR detections at natural abundance. The corresponding Larmor frequency was 55.1 MHz. A single-pulse sequence with a 31 μs long hard pulse was used, corresponding to a 45° pulse angle. The spectra were collected in 9000—30000 scans depending on the linewidth of the peaks, with an acquisition time of 60 ms and a recycle delay time of 0.6 s. Peak positions in the ^{25}Mg NMR spectra were referenced to the 1 M magnesium chloride ($MgCl_2$, 0 ppm) solution placed externally in the NMR spectrometer. Chemical shifts and linewidths of NMR signals were obtained by fitting Lorentzian functions to the experimental spectra using the NUTs processing environment (v.2012, Acorn NMR Inc., Las Positas, CA, USA). All NMR measurements were carried out at room temperature (20 °C).

2.1.3. Electrochemical evaluation

All electrochemical experiments were performed inside an Ar-filled glove box at room temperature using a CHI660C Potentiostat. The electrolytes were aged for at least 24 h prior to testing. The Mg deposition/stripping properties were evaluated using cyclic voltammograms and a three electrode configuration. The working electrode was a Pt electrode (1.0 mm diameter, PEEK-encased) and was polished prior to each experiment. The reference and counter electrodes were both freshly polished Mg metal strips. The voltage window was − 0.6–2.0 V vs. Mg and the scan rate was 20 mV/s. The voltammetry is generally stable for these electrolytes and the CV profiles reported in this paper

Table 1
The experimentally observed and the model free predicted chemical shifts of ^{25}Mg NMR along with the linewidth of the peak.

Label	Solute	Concentration(Mole/Mole)	$[BH_4]/[TFSI]$ ratio	Linewidth/Hz[a]	Exp.peak center (ppm)	Half peak positions (ppm)	Predicted (ppm)
a	$Mg(BH_4)_2$	0.01	1/0	150.15	13.5	14.86 12.14	13.5
b	$Mg(BH_4)_2/Mg(TFSI)_2$	0.01/0.001	10/1	194.58	12.2	13.97 10.43	12.3
c	$Mg(BH_4)_2/Mg(TFSI)_2$	0.01/0.0025	4/1	216.47	11.8	13.76 9.84	10.9
d	$Mg(BH_4)_2/Mg(TFSI)_2$	0.01/0.005	2/1	312.01	9.6	12.43 6.77	9.1
e	$Mg(BH_4)_2/Mg(TFSI)_2$	0.01/0.01	1/1	327.28	6.3	9.27 3.33	6.9
f	$Mg(BH_4)_2/Mg(TFSI)_2$	0.01/0.04	1/4	325.77	1.8	4.76 −1.16	2.9
g	$Mg(TFSI)_2$	0.4	0/1	332.74	0.3	3.32 −3.02	0.3

[a] An exponential filter equivalent to Lorentzian line broadening of 25 Hz was applied prior to Fourier transformation. The line width was measured at the half height positions of the peak in units of Hz.

are of the third deposition-stripping cycle. Note that if a voltage higher than 2 V is scanned, the electrolytes will be subject to oxiation owing to the low anodic stability of pure $Mg(BH_4)_2$ in DGM (1.7 V *vs.* Mg on Pt).

2.2. Computational details

2.2.1. Quantum chemistry calculations

Computational modeling of the NMR chemical shifts was carried out using the Amsterdam Density Functional (ADF-2013) package [49]. The generalized gradient approximation (GGA) based Becke-Lee-Yang-Parr [50,51] function with dispersion correction (BLYP-D)[52] was employed for geometry optimization. All calculations were carried out by using the TZ2P basis set (Triple ζ, 2 polarization function) with the Slater type functional [53] implemented in the ADF program. NMR calculations were performed based on the geometry optimized structures at the same level of the theory and with the same basis set to evaluate the chemical shielding for each atom. An ocatahedrally coordinated Mg^{2+} ion solvated by 6 water molecules was used as the computational reference as the known majority Mg^{2+} species of $MgCl_2$ in aqueous solution[46]. The chemical shielding predicted for $Mg^{2+}{\cdot}6H_2O$ is 565.2 ppm. The calculated ^{25}Mg chemical shielding can be converted to the experimentally observed scale by $\delta_{obs} = 565.2 - \delta_{calc}$ ppm. The utilization of BLYP-D was validated by the similar results (within numerical accuracy) obtained for representative molecules optimized with the more expensive hybrid B3LYPD (Table S1).

2.2.2. Molecular dynamics simulations

Classical molecular dynamics (MD) simulations were performed using the GROMACS MD simulation package version 4.5.3 to study solvation structures and dynamical properties [54]. Simulation details closely follow those described in our previous publication [55]. We first build a cubic simulation box of size $8 * 8 * 8\,nm^3$ with periodicity in XYZ direction. We considered 0.01 M concentration for $Mg(BH_4)_2$ mixed in 0, 0.001, 0.0025, 0.005, 0.01, 0.04 M $Mg(TFSI)_2$ in DGM to understand the effect of the additive $Mg(TFSI)_2$ in the solution. It should be pointed out that without $Mg(TFSI)_2$ the saturated concentration of $Mg(BH_4)_2$ in DGM is 0.01 M. Due to the prohibitively large simulation box and long computational time needed for very low concentration of salts, the ratio of the $Mg(BH_4)_2/Mg(TFSI)_2$ in DGM was kept similar to those in the NMR experiments but at higher salt concentration with 0.1 M $Mg(BH_4)_2$ mixed in 0, 0.1, 0.2, 0.3, 0.4 M $Mg(TFSI)_2$ in DGM for the residence time calculations. The force field parameters were obtained by computing partial charges with the RESP procedure by fitting the electrostatic potential surface of the optimized structure using Antechamber [56–58]. The bonded and non-bonded parameters were obtained using the generalized AMBER force field (GAFF) [56,57]. Lennard-Jones interactions were truncated at a cutoff distance of 1.2 nm. The particle-mesh Ewald (PME) method was used to handle long-range electrostatic interactions using a cutoff of 1.2 nm. The initial structures were then subjected to a two-step energy minimization, first using the steepest descent algorithm employing convergence criteria of 1000 kcal/mol Å and then using a conjugated-gradient minimization scheme with an energy convergence criteria of 10 kcal/mol Å. The two-step minimization allows for the release of strained contacts in the initial configurations. Isothermal-isobaric (NPT) simulations were performed to obtain the correct density on the minimized system using a Berendsen barostat to maintain the pressure of 1 atm for 2 ns [59]. All systems were then melted to 400 K for 2 ns and then subsequently annealed to 298 K in three steps for 3 ns. Afterward, canonical ensemble (NVT) simulations were performed for 10 ns at 298 K using an improved velocity-rescaling algorithm with a coupling constant of 0.1 ps to equilibrate and sample the properties of interests. We took the final configuration from the NVT ensemble and repeated the above steps (melting, annealing, and equilibration) at least one more time. All of our reported results were averaged over two independent NVT production runs of the same system.

3. Results and discussion

The fundamental understanding of the correlation between the solvation structure and the dynamical properties of ionic species in a multicomponent mixture and its effect on the electrochemical properties provides an important basis for designing optimized electrolytes. Here, we used MD simulations and NMR to understand the solvation structure and transport properties of neat $Mg(BH_4)_2$/DGM and neat $Mg(TFSI)_2$/DGM solutions as well a more complex $Mg(BH_4)_2$ + $Mg(TFSI)_2$ in DGM solution as a function of concentration of $Mg(TFSI)_2$. Fig. 1a shows the ^{25}Mg NMR spectra of 0.01 M $Mg(BH_4)_2$ and a variable concentration of $Mg(TFSI)_2$ ranging from 0 to 0.04 M dissolved in DGM. The ^{25}Mg chemical shift of pure 0.01 M $Mg(BH_4)_2$ (corresponding to the saturated concentration in DGM) is at 13.5 ppm (Fig. 1a(a)) while that of pure 0.4 M $Mg(TFSI)_2$ is located at 0.3 ppm (Fig. 1a(g)). Note that the ^{25}Mg NMR chemical shifts for pure $Mg(TFSI)_2$ dissolved in DGM with concentrations varying from 0.005 M to 0.4 M are essentially the same, i.e., at about 0.3 ppm (see Fig. S1 in the Supporting Information). For the mixture with both $Mg(BH_4)_2$ and $Mg(TFSI)_2$, a single broad peak is observed in all cases studied (Fig. 1a(b-f)), strongly indicating the presence of either i) a single solution structure or ii) a convolution of multiple solution structures with rapid exchange. Examining the solution as a function of different salt concentrations, we find that peak positions as well as their widths evolve. The chemical shift value of the peak center decreases monotonically with the increasing concentrations

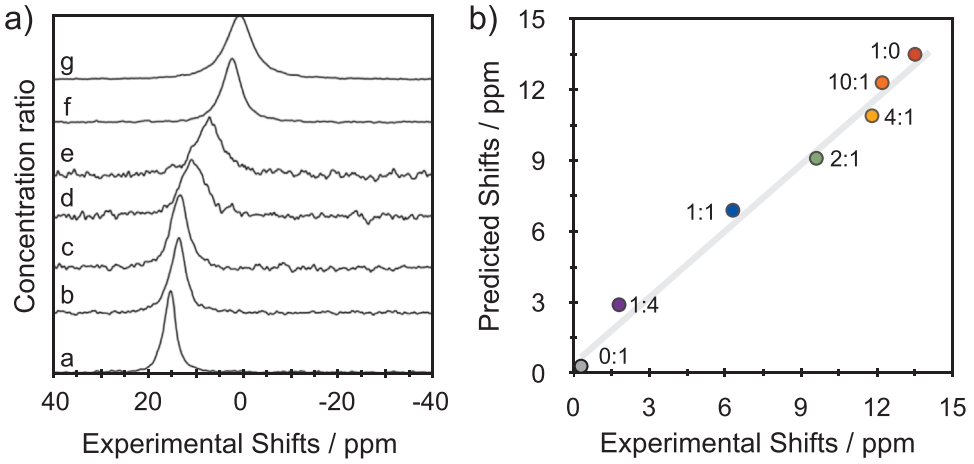

Fig. 1. a) ^{25}Mg NMR spectra of $Mg(BH_4)_2$ and Mg $(TFSI)_2$ dissolved in DGM with different concentrations of ($Mg(BH_4)_2$: $Mg(TFSI)_2$). (a) 0.01 M : 0 M; (b) 0.01 M : 0.001 M; (c) 0.01 M : 0.0025 M; (d) 0.01 M: 0.005 M; (e) 0.01 M : 0.01 M; (f) 0.01 M: 0.04 M; (g) 0 M : 0.4 M. b) correlation between the predicted chemical shifts and experimental results. The labels on the points are the molar ratios of $Mg(BH_4)_2$: Mg $(TFSI)_2$.

of $Mg(TFSI)_2$. For the mixture with 0.01 M $Mg(BH_4)_2$ and 0.001 M Mg $(TFSI)_2$, the peak center is located at 12.2 ppm, already shifted away from that the value of 13.5 ppm measured for pure 0.01 $Mg(BH_4)_2$. For the mixture with 0.01 M $Mg(BH_4)_2$ and 0.04 M $Mg(TFSI)_2$, the peak center shifts to 1.8 ppm, approaching the value of 0.3 ppm found for pure 0.4 M $Mg(TFSI)_2$. In contrast, the line width – defined as the width at the half peak height positions – is the narrowest (150 Hz) for pure 0.01 M $Mg(BH_4)_2$, then gradually increases with the concentration of $Mg(TFSI)_2$ and finally reaches 333 Hz for the case of pure 0.4 M Mg $(TFSI)_2$. In view of this evidence, a single solvation structure is unlikely. We deduce that the decreased chemical shift values and the increased peak widths as a function of the increasing concentration of $Mg(TFSI)_2$ consistently support a fast molecular exchange between at least two solvation structures. Following the simplest version of this hypothesis, we assume two distinct solvation structures, i.e., **Structure-A,** for pure 0.01 M $Mg(BH_4)_2$ in DGM and **Structure-B** for 0.04 M pure $Mg(TFSI)_2$ in DGM (structures defined below). We further hypothesize that if the exchange rate between **Structure-A** and **Structure-B** is much faster than the difference of the peak centers in units of Hz, i.e., greater than $(13.5 - 0.3) \times 55.1 = 727.32$ Hz, a single ^{25}Mg NMR peak will be observed experimentally. To verify this hypothesis, a linear correlation between the predicted chemical shifts using the known concentrations of $Mg(BH_4)_2$ and $Mg(TFSI)_2$ and the experimentally observed chemical shifts must be proven. Under the condition of fast exchange, the chemical shift (δ_m) in a mixed electrolyte is predicted with the experimental results of 0.01 M $Mg(BH_4)_2$ and that of $Mg(TFSI)_2$ according to the equation

$$\delta_m = c_1/(c_1 + c_2) \times \delta_1 + c_2/(c_1 + c_2) \times \delta_2 \quad (1)$$

where $\delta_1 = 13.5$ ppm, $\delta_2 = 0.3$ ppm, and c_1 and c_2 are either the concentrations or the molar ratios of $Mg(BH_4)_2$ and $Mg(TFSI)_2$ respectively (See Table 1). For example, in the case that the ratio of $[BH_4]/[TFSI]$ is 10/1, the concentrations of $Mg(BH_4)_2$ and $Mg(TFSI)_2$ are 0.01 M and 0.001 M respectively. Based on Eq. (1), the predicted chemical shift under fast molecular exchange between **Structure-A** and **Structure-B** is 12.3 ppm. The predicted results for all other concentrations are summarized in Table 1. Comparing with the experimental results, the differences are less than 1.1 ppm, so the predicted values are highly consistent with the experimental results. As further verification, the experimental and predicted results are summarized in a correlation diagram as shown in Fig. 1b. We obtain a correlation coefficient, r of 0.994, between the predicted and the experimental shifts, indicating a highly linear correlation that supports the existence of fast molecular exchange between the two solvation structures (**Structure-A** and **Structure-B**.)

3.1. Solvation structure and the mechanisms of molecular exchange

We used classical MD simulations to further elucidate the mechanism behind the evolving solvation structures of neat $Mg(BH_4)_2$-DGM, $Mg(TFSI)_2$-DGM and the more complex $Mg(BH_4)_2$ + $Mg(TFSI)_2$ in DGM solutions. Fig. 2a and b show the radial distribution function (RDF) of the 0.01 M $Mg(BH_4)_2$ in DGM and 0.04 M $Mg(TFSI)_2$, respectively. It is observed that there is a very strong interaction between Mg^{2+} and BH_4^- as indicated by the first sharp peak of Mg-B(BH_4) observed at 2.2 Å. This strong interaction precludes solvent (DGM) mediated dissociation of Mg^{2+} and BH_4^- in the solution and results in the formation of contact ion pairs even at low concentration of 0.01 M. We observed a coordination number (CN) of 2.1 for Mg-BH_4 and 1.8 for Mg-DGM (Fig. 2c) indicating that each Mg^{2+} ion is surrounded by two BH_4^- and one to two DGM molecules in the first solvation shell for tridentate (Fig. 3a or Fig. S3) and mono or bi-dentate coordination of DGM respectively. Such strong interaction between Mg^{2+} and BH_4^- results in extremely low solubility of $Mg(BH_4)_2$ salt in DGM.

The presence of contact ion pairs in $Mg(BH_4)_2$ was also observed in previous experimental and simulation studies [60,61]. Fig. 3a shows the optimized geometry of $Mg(BH_4)_2$/DGM from first-principles DFT calculations using the methods detailed in the Quantum Chemistry Calculation of the Computational Details of the Methodology Section, where two hydrogen atoms from each of the two BH_4^- groups are bonded to the Mg atom, and a DGM molecule coordinates a Mg^{2+} ion with three oxygen atoms [38]. By considering only the first solvation shell in quantum calculations, we obtained a calculated ^{25}Mg chemical shift of 21.2 ppm, which is quite different from the experimental result of 13.5 ppm (Fig. 1a). Based on the coordination number of Mg-DGM in the second solvation sphere obtained from MD simulations, up to 6 DGM molecules were added as the second solvation shell in quantum calculations of ^{25}Mg chemical shift. To examine the effect of varying number of DGM molecules, Fig. 3b and c show models containing three and five DGM molecules in the second solvation shell. The corresponding calculated ^{25}Mg chemical shifts are 18.1 ppm and 13.3 ppm respectively (Table 2), which indicates that DGM molecules in the second shell have a significant effect on the calculated Mg^{2+} chemical shift. A good agreement with the experimental NMR result of 13.5 ppm is reached, consistent with the MD results, for five DGM molecules. The calculated ^{25}Mg chemical shift of 15.7 (Table 2) for six DGM in the second solvation shell is also close to the experimental value of 13.5 ppm. Therefore, from combined NMR, MD and first-principles calculations, we propose that the solvation structure of 0.01 M Mg $(BH_4)_2$ dissolved in DGM is comprised of two BH_4^- anions and one DGM molecule in the first solvation shell of Mg^{2+}, while there are five to six DGM molecules in the second solvation shell, Structure-A. For the 0.04 $Mg(TFSI)_2$/DGM solution, the first radial distribution function peak in

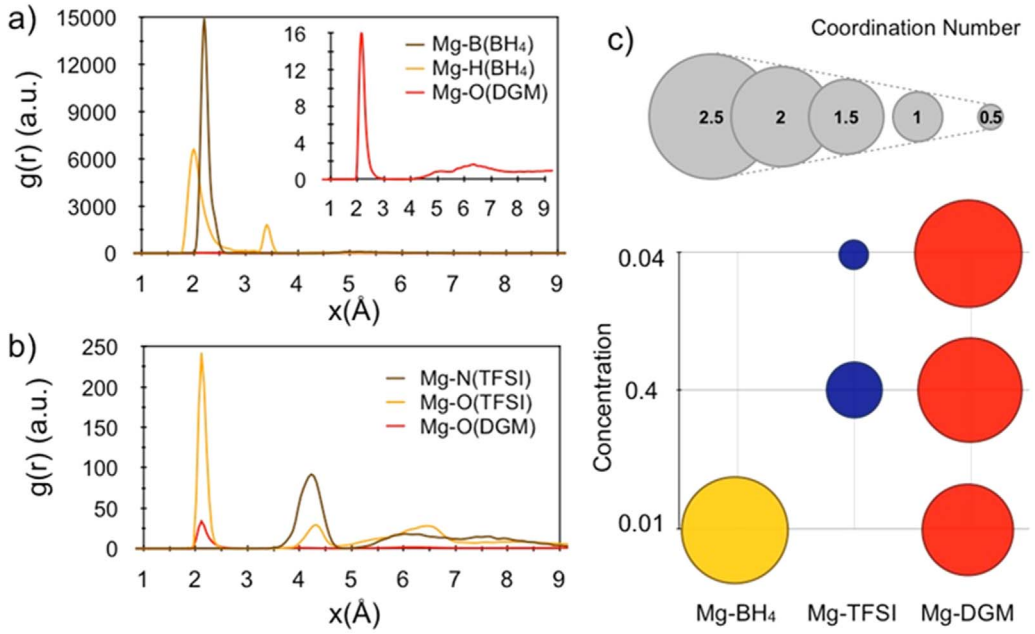

Fig. 2. Radial distribution function of a) Mg-B(BH_4), Mg-H(BH_4), and Mg-O(DGM) in 0.01 M $Mg(BH_4)_2$/DGM b)Mg-N(TFSI), Mg-O(TFSI), Mg-O(DGM) in 0.04 M $Mg(TFSI)_2$/DGM c) coordination number computed for Mg-BH4, Mg-TFSI, Mg-DGM in the first solvation shell around Mg^{2+}.

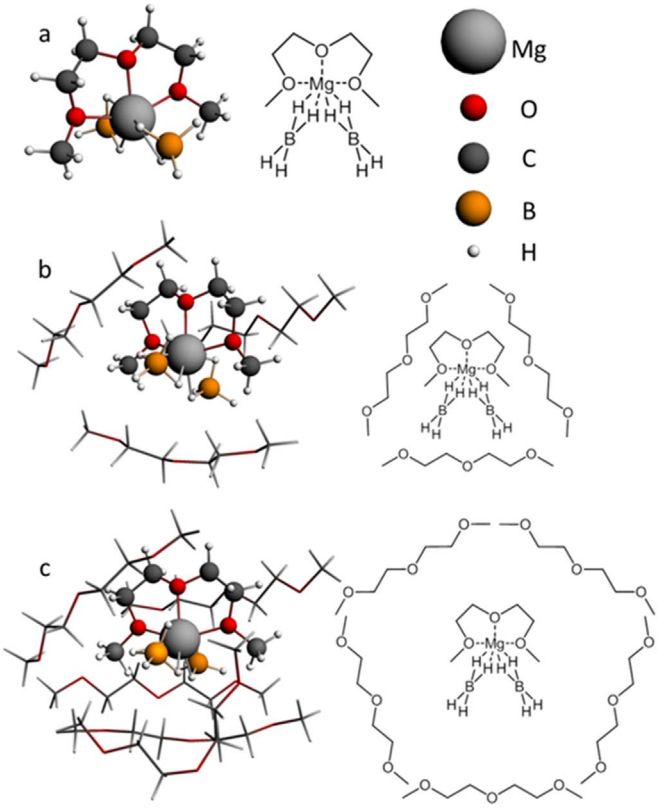

Fig. 3. DFT-optimized predictions of the solvation structures of $Mg(BH_4)_2$ dissolved in DGM. (a) $Mg(BH_4)_2$DGM; (b) $Mg(BH_4)_2(DGM)_4$; (c) $Mg(BH_4)_2(DGM)_6$. $Mg(BH_4)_2(DGM)_6$ provides DFT-predicted chemical shifts in good agreement with experimental results and is designated as Structure-A.

the solvation structure around Mg^{2+} is observed from the oxygen atoms of $TFSI^-$ and DGM at ~ 2.1 Å and the peak from nitrogen of $TFSI^-$ is observed further at a distance of ~ 4.3 Å (Fig. 2b). The coordination number of Mg-TFSI is 0.27 at 0.04 M and 1.1 at 0.4 M indicating the presence of solvent separated ion pairs at 0.04 M and contact ion pairs at 0.4 M concentration of $Mg(TFSI)_2$. The high oxygen donor denticity and flexibility of DGM allows complete dissociation of Mg-TFSI at lower concentration and the formation of contact ion pairs at 0.4 M concentration (Fig. 4) with one $TFSI^-$ anion in the first solvation shell around Mg^{2+}, forming solvation structures between 0.8 and 1.2 nm in diameter. Such increases in ion association which result in contact ion pair formation with an increase in the concentration of $Mg(TFSI)_2$ in DGM solvent has also been observed in previous studies [62]. For NMR peak calculations from first-principles, we first considered only the first solvation shell where Mg^{2+} is coordinated with one $TFSI^-$ anion and two DGM molecules. Four representative conformations after geometry optimization are depicted in Fig. 4. The calculated chemical shifts are 0.2 ppm, − 5.3 ppm, − 0.3 ppm and − 6.4 ppm for the structures in Fig. 4a, b, c, and d, respectively (Table 2). The calculated chemical shifts follow an upfield trend with an increase of the number of coordinated oxygen atoms. Among them, the value of 0.2 ppm (Fig. 4a) is in excellent agreement with the experiment of 0.3 ppm (Table 1), and the value of − 0.3 ppm (Fig. 4c) is also close to the experimental value. To consider the contributions from the second solvation shell, varying numbers of DGM were added to the two most likely conformations (Fig. a and c). Hence, two, four, and six DGM molecules are added into the structure in Fig. 4a to construct the second solvation shells (Fig. 5a-c). The corresponding calculated chemical shifts are 1.2 ppm, 1.2 ppm, and

Table 2
Calculated ^{25}Mg chemical shifts.

Label	Structures	^{25}Mg Chemical Shifts/ppm
Fig. 3a	$Mg(BH_4)_2$ DGM	21.2
Fig. 3b	$Mg(BH_4)_2$ DGM − 3DGM	18.1
Fig. 3c	$Mg(BH_4)_2$ DGM − 5DGM	13.3
	$Mg(BH_4)_2$DGM − 6DGM	15.7
Fig. 4a	$[MgTFSI]^+$ − 2DGM	0.2
Fig. 4b	$[MgTFSI]^+$ − 2DGM	− 5.3
Fig. 4c	$[MgTFSI]^+$ − 2DGM	− 0.3
	$[MgTFSI]^+(2DGM)_2$ − 2DGM	− 1.7
	$[MgTFSI]^+(2DGM)_2$ − 4DGM	− 3.8
Fig. 4d	$[MgTFSI]^+$ − 2DGM	− 6.4
Fig. 5a	$[MgTFSI]^+(DGM)_2$ − 2DGM	1.2
Fig. 5b	$[MgTFSI]^+(DGM)_2$ − 4DGM	1.2
Fig. 5c	$[MgTFSI]^+(DGM)_2$ − 6DGM	1.6

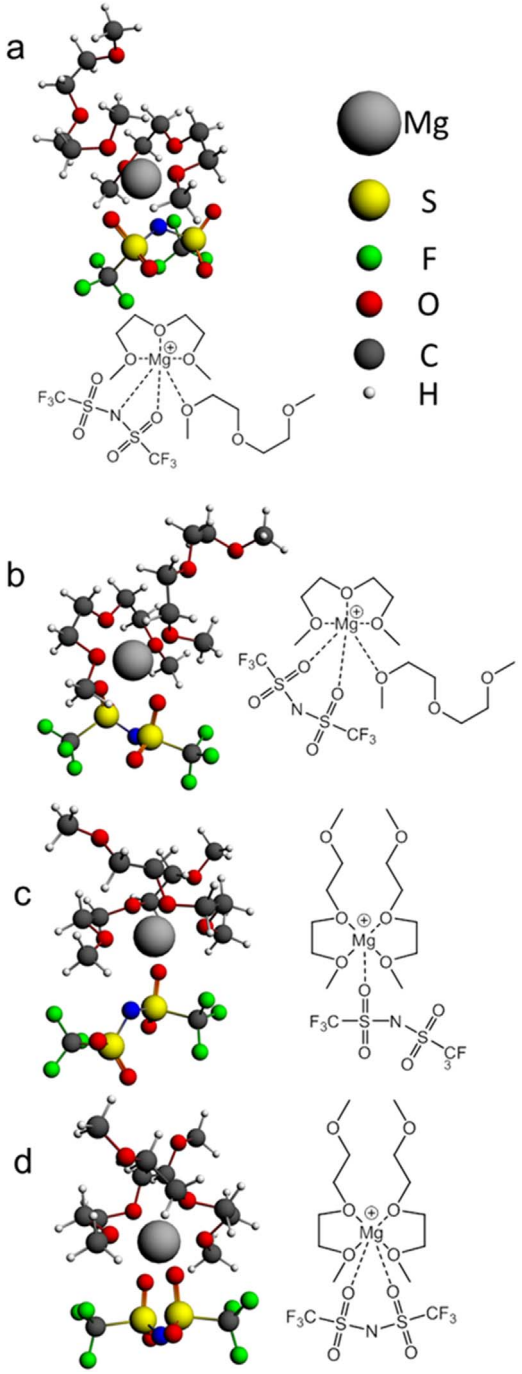

Fig. 4. Several proposed first solvation structures of $[MgTFSI]^+ - 2DGM$. The first conformation, a, agrees best with experimental results and is likely the solvation structure for the first shell in Structure-B.

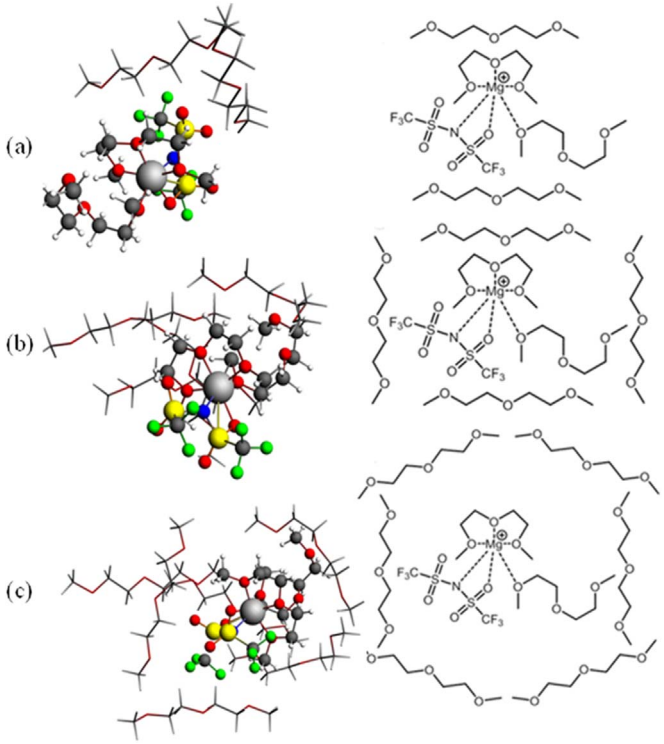

Fig. 5. $[MgTFSI]^+ - 2DGM$ with both first and second solvation shells. The second solvation shell has a limited impact on the shielding of the Mg atom, and thus a, b, and c are all candidates for Structure-B.

1.6 ppm, respectively (Table 2) which are all in reasonable agreement with the experimental value of 0.3 ppm considering the broad shape of the ^{25}Mg NMR peak, i.e., the half peak heights at 3.3 ppm and − 2.7 ppm. Similarly, two, and four DGM molecules are added into the structure in Fig. 4c to construct the second solvation shells, and the corresponding calculated chemical shifts are − 1.7 ppm, and − 3.8 ppm, respectively. Considering both the NMR and MD results, we find that the of the multiple conformers of the first solvation structure for the system $Mg(TFSI)_2$-DGM is $[MgTFSI]^+ - 2DGM$, Fig. 4a is the most probable structure for Structure-B. We also find that adding the second solvation shell containing two or four DGM molecules causes only minor changes (less than about 0.9 ppm) to the predicted chemical shift value of Mg for this structure while expanding the overall solvation structure from about 1.2–1.6 nm.

At very dilute $Mg(TFSI)_2$ concentrations in DGM, there is also a possibility that $TFSI^-$ is completely dissociated from Mg^{2+} based on the MD results above. This possibility is explored for a variety of models where a Mg^{2+} is coordinated by a different number of DGM molecules. The results of the cluster models that generate predicted chemical shifts close to the experimental values are summarized in Fig. S4 of the Supplementary Information. Two first-solvation structures, involving 2 and 3 DGM molecules respectively, generate ^{25}Mg chemical shifts of − 1.7 ppm for $Mg(DGM)_3$ and − 3.6 ppm for $Mg(DGM)_2$ (Table S2) close to the experimental values of 0.3 ppm. In both cases, a Mg^{2+} interacts with six oxygen atoms from either two (i.e., each donating three oxygens in the case of $Mg(DGM)_2$) or three (each donating two oxygens in the case of $Mg(DGM)_3$) DGM molecules. Adding second solvation shells containing two to six DGMs on these two basic first solvation shell structures can further improve the agreement between the calculated chemical shifts and the experimentally observed shift. For example, for $Mg(DGM)_2$ with 4 DGMs ($Mg(DGM)_2(DGM)_4$ in Table S2) in its second shell a ^{25}Mg chemical shift of 1.1 ppm is calculated that is even closer to the experimental value of 0.3 ppm. Likewise, for $Mg(DGM)_3$ with either two DGMs ($Mg(DGM)_3(DGM)_2$), four DGMs ($Mg(DGM)_3(DGM)_4$), or six DGMs ($Mg(DGM)_3(DGM)_6$) in the second shell, − 0.8 ppm, 1.7 and 1.8 ppm peaks are predicted, respectively (Table S2). These predicted values are also close to the experimental value of 0.3 ppm given the broad line width of the $^{25}Mg^{2+}$ peak (Table 1 and Fig. S1). Therefore, at dilute concentration in DGM there exists the possibility of Mg^{2+} that is completely disassociated from $TFSI^-$, with the flexibility of multiple conformations, which provides another candidate for **Structure-B** at very dilute $Mg(TFSI)_2$ concentrations in DGM.

In order to understand the effect of two competing anions on the solvation structure, we studied the solvation structure of mixtures containing both $Mg(BH_4)_2$ and $Mg(TFSI)_2$ dissolved in DGM. Fig. 6a shows the radial distribution function of Mg-BH_4 as a function of the concentration of $Mg(TFSI)_2$. We observed a single peak at ~ 2.2 Å in

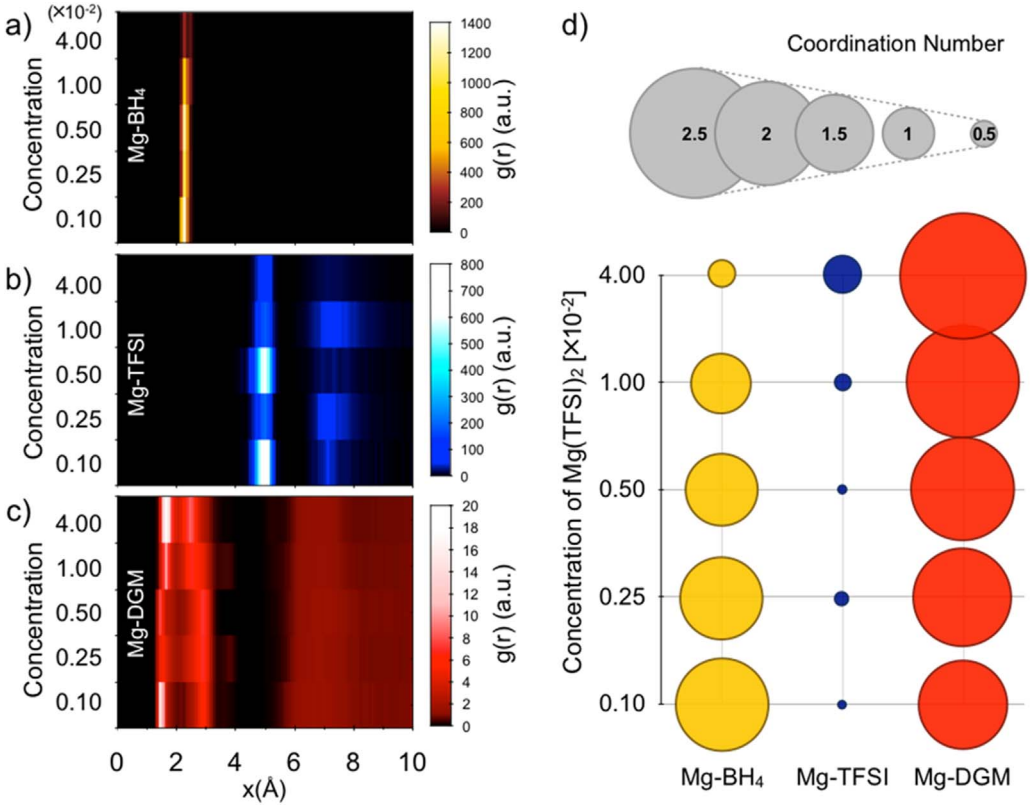

Fig. 6. Radial distribution function of a) Mg-BH_4 b) Mg-TFSI c) Mg-DGM and d) coordination number Mg-BH_4, Mg-TFSI, Mg-DGM in a mixed solution of 0.01 M $Mg(BH_4)_2$/DGM and varying concentration of $Mg(TFSI)_2$. The y-axis shows the concentration of $Mg(TFSI)_2$ in the solution.

agreement with the neat solution but the peak intensity decreases significantly with increasing concentration of $Mg(TFSI)_2$ in the solution (Fig. 2b). The competing interaction from the $TFSI^-$ anion to coordinate with Mg^{2+} results in a stronger intensity of the Mg-TFSI RDF peak with an increased concentration of $Mg(TFSI)_2$. This competing interaction between the two anions disrupts the rigid solvation structure of Mg-BH_4 and allows more solvent molecules to interact with Mg^{2+}, which in turn increases the solubility of the $Mg(BH_4)_2$ salt. The effect of this change in the solvation structure as a function of $Mg(TFSI)_2$ concentration in 0.01 M $Mg(BH_4)_2$/DGM solution can also be observed in the coordination number of Mg-BH_4 as it decreases from 1.8 to 0.5 with an increase in $Mg(TFSI)_2$ concentration from 0.001 to 0.04 M. Hence the formation of contact ion pairs of Mg-BH_4 in neat $Mg(BH_4)_2$/DGM solution and in mixtures with very small concentration of $Mg(TFSI)_2$ become favorable, while partially solvent separated ion pairs of Mg-BH_4-TFSI, where TFSI is entering into the first solvation shell, are formed at higher concentrations of $Mg(TFSI)_2$. As $TFSI^-$ is a weakly coordinating anion, the increase in Mg-TFSI coordination number is not significant and solvent separated ion pairs of Mg-TFSI from even at the highest examined concentration of $Mg(TFSI)_2$ (0.04 M). On the other hand, a significant increase was observed in the coordination number of Mg-DGM with increased $Mg(TFSI)_2$ concentration, which would enhance the solubility of $Mg(BH_4)_2$ solution as discussed previously. Stable Mg species are observed in mixed Mg electrolyte [Mg-BH_4-TFSI]/DGM solution, where both the BH_4^- and $TFSI^-$ enter into the first solvation shell of Mg^{2+} in the mixed electrolyte systems (Fig. 7). Such a solvation structure can potentially reduce the risk of charge-transfer mediated $TFSI^-$ decomposition which was previously proposed for $Mg(TFSI)_2$ [10,61]. Furthermore, a weaker interaction between Mg^{2+} and BH_4^- may also enhance the ionic conductivity and the electrochemical performance as suggested previously by Mohtadi et al.[60] Based on coordination numbers obtained from MD simulation, we computed the ^{25}Mg NMR shift for the structure containing one DGM molecule chelating one Mg^{2+} plus one BH_4^- and one $TFSI^-$. $TFSI^-$ is known to exist in multiple conformers in solution so here we considered three possible coordinations of the $TFSI^-$ anion. They are labeled in Table S3 as $Mg(BH_4)$(TFSI)(DGM-1) for the trans-conformer of $TFSI^-$ where it donates one oxygen atom to Mg^{2+}, $Mg(BH_4)$(TFSI)(DGM) − 2 for the trans-conformer of TFSI where the Mg^{2+} is bonded to one oxygen atoms from the SO_2 group and the nitrogen, and $Mg(BH_4)$(TFSI)(DGM-3) for the cis-conformer of TFSI where the Mg^{2+} is bonded to two oxygen atoms from each SO_2 group. The predicted ^{25}Mg chemical shifts are 17.0 ppm for $Mg(BH_4)$(TFSI)DGM-1, 5.5 ppm for $Mg(BH_4)$(TFSI)DGM-2, − 4.6 ppm for $Mg(BH_4)$(TFSI)DGM-3 and − 5.2 ppm for $Mg(BH_4)(TFSI)_2DGM^-$, respectively (Table S3). Only the value of 5.5 ppm falls within the observed experimental values between 0.3 ppm and 13.5 ppm (see Table 1) for the mixtures with varied ratios of $Mg(BH_4)_2$ and $Mg(TFSI)_2$ in DGM. Adding second solvation shells containing 1–5 DGM molecules onto the above three types of first shell solvation structures can impact the predicted ^{25}Mg NMR chemical shifts. These results are also summarized in Table S3 of Supporting Information. However, only the Mg(BH_4)(TFSI)DGM-2 structure results in shifts within the observed experimental range; 7.4 ppm for one DGM, 4.8 ppm for three DGMs, and 3.3 ppm for five DGMs in the second solvation shell. These results indicate that the solvation shell structure of $Mg(BH_4)$(TFSI)DGM-2 (**Structure-C**) along with its various second solvation structures reported here are the structures that facilitate the exchange between **Structure-A** and **Structure-B. Structure-C,** i.e., $Mg(BH_4)$(TFSI)DGM-2 with five DGMs in its second solvation shell, is most likely the dominant solvation structure for the mixture at high salt concentrations. These configurations are presented in Fig. 7a-d. This assignment is justified by using the experimental ^{25}Mg NMR spectra obtained on systems of 0.1 M $Mg(BH_4)_2$ + 0.1 M $Mg(TFSI)_2$, 0.1 M $Mg(BH_4)_2$ + 0.2 M $Mg(TFSI)_2$, and 0.1 M $Mg(BH_4)_2$ + 0.3 M $Mg(TFSI)_2$ in Fig. S2. Fig. S4 displays the ^{25}Mg NMR peak centers at approximately 2.2, 1.7 and 1.0 ppm for the systems of 0.1 M $Mg(BH_4)_2$ + 0.1 M $Mg(TFSI)_2$, 0.1 M $Mg(BH_4)_2$ + 0.2 M

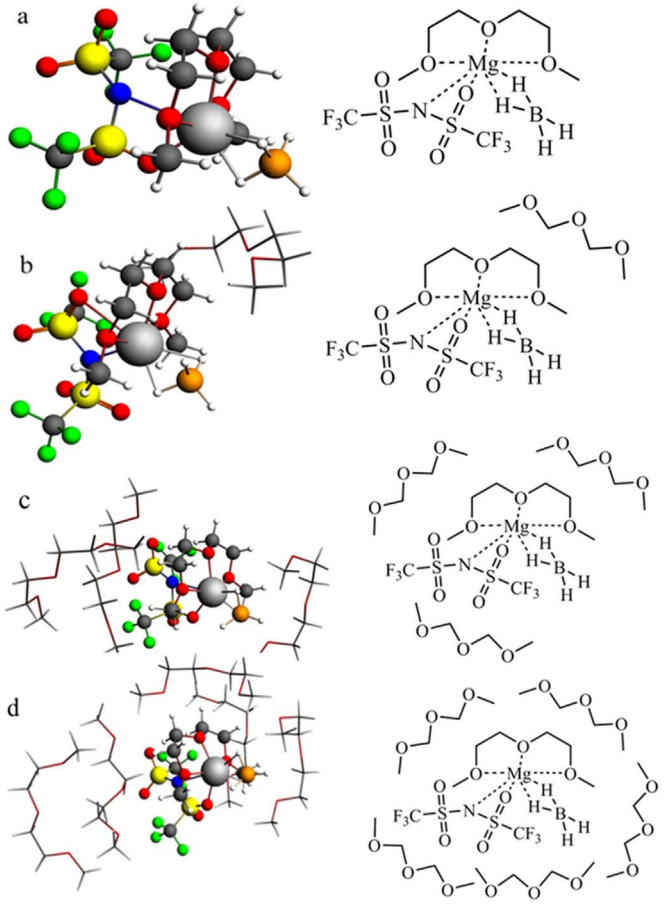

Fig. 7. DFT-optimized structures representing Structure-C with a) 0, b) 1, c) 3, and d) 5 DGM molecules in the second solvation shell.

$Mg(TFSI)_2$, and 0.1 M $Mg(BH_4)_2$ + 0.3 M $Mg(TFSI)_2$, respectively. Calculations using ADF predicted a ^{25}Mg NMR chemical shift for **Structure-C** of 3.3 ppm. By assuming a fast molecular exchange between **Structure-C** (3.3 ppm) and **Structure-B** (0.3 ppm), we can calculate/predict the ^{25}Mg chemical shifts by using Eq. (1). We obtain ^{25}Mg chemical shifts of 1.8, 1.3 and 1.1 ppm for the systems of 0.1 M $Mg(BH_4)_2$ + 0.1 M $Mg(TFSI)_2$, 0.1 M $Mg(BH_4)_2$ + 0.2 M $Mg(TFSI)_2$, and 0.1 M $Mg(BH_4)_2$ + 0.3 M $Mg(TFSI)_2$, respectively. These calculated values are in good agreement with the experimental results of 2.2, 1.7 and 1.0 ppm for the corresponding systems, suggesting that (i) **Structure-C** is an excellent candidate for the dominant solvation structure for the mixture in DGM with both high $Mg(BH_4)_2$ and high $Mg(TFSI)_2$ concentrations of equal or greater than 0.1 M; and (ii) fast molecular exchange occurs between **Structure-C** and **Structure-B.**

Hence, two possible mechanisms can be proposed to explain the fast exchange between **Structure-A** and **Structure-B** observed in NMR at dilute mixed salt concentrations (Table 1) of $Mg(BH_4)_2$ and $Mg(TFSI)_2$ in DGM. The first one is a gradual exchange of the BH_4^- for $TFSI^-$ in the first solvation shells, plus the rearrangement of DGM orientation in the second solvation shells such that **Structure-A** becomes **Structure-B**. This process can be facilitated via **Structure-C**. The second mechanism is a direct exchange of Mg-ions between **Structure-A** and **Structure-B** with a residence time less than about 1/727.32 Hz = 1.4 ms. In this case, the Mg-ions in both structures need to break the bonding of the tridentate ligand of DGM.

To estimate the lifetime of anions and solvent molecules in the first solvation shell of Mg^{2+} we computed the residence time between the anion and solvent molecules associated with the cation using a residence correlation function [63]

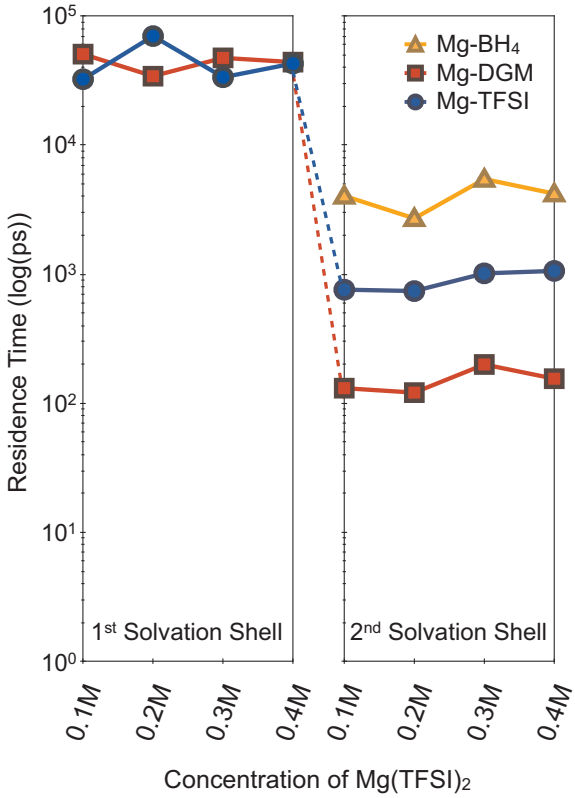

Fig. 8. Residence time of Mg-BH_4^-, Mg-DGM and Mg-TFSI in first (left) and second (right) solvation shell around Mg^{2+} at a constant concentration of 0.1 M $Mg(BH_4)_2$ and varied concentration of $Mg(TFSI)_2$ in DGM. The residence time of BH_4^- in the first solvation shell is not shown, as it did not converge during the length of trajectory (i.e., 20 ns) considered in this work.

$$P(t) = \frac{\langle S_{ij}(t)\rangle\langle S_{ij}(0)\rangle}{\langle S_{ij}(0)S_{ij}(0)\rangle}, \quad (2)$$

where $S_{ij}(t)$ is equal to 1 when the neighbor **j** (TFSI, BH_4, DGM) is within the solvation shell of **i** (Mg^{+2}), otherwise S_{ij} is 0, where $\langle\ \rangle$ denotes the average over all pairs and reference times. When P(t) reaches zero the neighbors defined at the reference time have been decorrelated. The time required for this occurrence is quantified [63] through assuming that

$$P(t) = e^{-\frac{t}{\tau}}. \quad (3)$$

Fitting Eq. (2) with Eq. (3), the residence time (τ) can be calculated between Mg^{+2} and its neighbors (BH_4^-, $TFSI^-$ and DGM). Therefore, the residence times for pairs within the first and second solvation shells, as defined by the RDFs in Fig. 2a-b, were computed using Eq. (2) over a 20 ns long trajectory with snapshots every 50 ps (Fig. 8). It is observed that the residence times of $TFSI^-$ and DGM in the first solvation shell are comparable, which suggest that both $TFSI^-$ and DGM spend similar time in the first solvation shell of Mg^{2+}, indicating approximately equivalent interactions with Mg^{2+}. The residence time of BH_4^- in the first solvation shell is not shown in Fig. 8 as it remained correlated during the 20 ns simulation time. This is not surprising as we observed very strong interaction through H-bonding between BH_4^- and Mg^{2+} in the solvation structure of neat $Mg(BH_4)_2$ in DGM. Hence, the residence time of BH_4^- in the first solvation shell around Mg^{2+} is estimated to be much longer than those of $TFSI^-$ and DGM, and we deduce that the hopping of Mg^{2+} ions between solvation **Structure A** and **B** is unlikely to happen on a 100 ns time scale. Note that it is not currently feasible to simulate a time scale close to or beyond 100 ns for the large simulation box considered in this work. In the second solvation shell, the anions exhibit residence times corresponding to approximately 4–5 ns for BH_4^- and

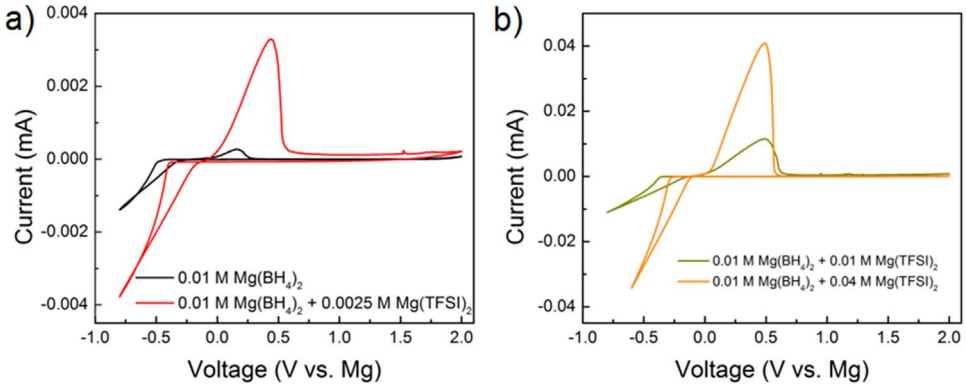

Fig. 9. Cyclic voltammetry of electrolyte solutions prepared in diglyme with different concentrations of $Mg(BH_4)_2$ and $Mg(TFSI)_2$ as labeled. The scan rate was 20 mV/s.

~1 ns for TFSI. In contrast, DGM exhibits short residence times between 131 and 200 ps, which indicates fast movements and weak interaction with Mg^{2+}. Hence, we find that the DGM molecules in the second solvation shell rearrange themselves efficiently by switching between **Structure-A** and **Structure-B**. This process combined with identification of intermediate **Structure-C** makes possible a gradual change from **Structure-A** to **Structure-B** and vice versa. In this context we note that previous studies have also shown that the diffusion of cations are faster through structural diffusion with ions or via a solvent exchange mechanism [63]. Such fast exchange improves the dynamics of the electrolyte and hence the conductivity.

4. Electrochemical evaluation of the composite electrolytes

We find that the salt ratios of the electrolytes have pronounced effects on the Mg deposition and stripping properties. Fig. 9 compares the cyclic voltammetry (CV) curves acquired with each electrolyte at a scan rate of 20 mV/s. The results were analyzed and the activities are listed in Table 3, which shows that the pure $Mg(BH_4)_2$ electrolyte (saturated, ~ 0.01 M) exhibits very weak activities for Mg deposition, and both the Mg deposition current density and the Coulombic efficiency (15%) were quite low. The activities showed gradual improvements with the addition and increase of the concentration of $Mg(TFSI)_2$. The Coulombic efficiency, for example, increased from the 15% without $Mg(TFSI)_2$ to 55%, 75% and 89% at $Mg(TFSI)_2$ concentrations of 0.0025 M, 0.01 M and 0.04 M, respectively. Overall, we identified that the combination of 0.01 M $Mg(BH_4)_2$ and 0.04 M $Mg(TFSI)_2$ exhibited the best activity for Mg deposition and the current density was the highest. At this particular ratio, the presence of both $Mg(BH_4)_2$ and $Mg(TFSI)_2$ results in formation of solvent separated ion pairs as well as stable a structure with both BH_4 and TFSI anions in the first solvation shell. Improved Coulombic efficiency at increased $Mg(TFSI)_2$ concentrations has also been found for electrolyte solutions prepared with two high salt Mg $(BH)_4$ (0.1 M) and $Mg(TFSI)_2$ (0.1 or 0.2 M) combinations in DGM (Table S3). In summary, these electrochemistry data, together with the ^{25}Mg NMR and the simulation results, clearly shows that the Mg coordination environment exerts a strong influence on the performance of the electrolyte.

Table 3
Summary of electrochemical results of electrolyte solutions prepared with different salt combinations.

$Mg(BH)_4$	$Mg(TFSI)_2$	Overpotential (V)	Coulombic Efficiency
.01	0	0.25	15%
0.01	0.0025	0.25	55%
0.01	0.01	0.24	75%
0.01	0.04	0.16	89%

5. Conclusion

Our results indicate that even a small addition of $Mg(TFSI)_2$ to $Mg(BH_4)_2$ dissolved in diglyme (DGM) can significantly disrupt the well-defined solvation structure and strong interaction between Mg and BH_4, thus increasing the fraction of freely coordinated anions and resulting in significantly increased solubility of $Mg(BH_4)_2$ in DGM. This not only greatly enhances the dynamics but also improves the stability of the otherwise unstable TFSI anion. By taking advantage of the increased sensitivity using a combination of high magnetic field and a large sample volume probe, natural abundance ^{25}Mg NMR spectra of $Mg(BH_4)_2$ and $Mg(TFSI)_2$ dissolved in DGM at magnesium concentration as low as 10 mM were successfully acquired. Coupled with classical dynamics modeling, quantum chemistry calculations of ^{25}Mg NMR chemical shifts, the solvation mechanisms of $Mg(BH_4)_2$ and $Mg(TFSI)_2$ dissolved in DGM at various concentrations and ratios of $Mg(BH_4)_2$/$Mg(TFSI)_2$ were investigated. It was found that for the system of 0.01 M (saturated concentration) pure $Mg(BH_4)_2$ dissolved in DGM, there are two BH_4^- anions and one DGM molecules in the first solvation shell of a Mg^{2+} ion, while there are five to six DGM molecules in the second solvation shell (termed as **Structure-A**). For the system of pure $Mg(TFSI)_2$ in DGM, the first solvation shell of one preferred structure contains two DGM molecules and one TFSI anion while the second solvation shell contains approximately four DGM molecules (termed as **Structure-B**). At very dilute $Mg(TFSI)_2$ concentration in DGM there also exists the possibility of completely dissociated Mg^{2+} from $TFSI^-$, with the flexibility of multiple conformations, which provides another candidate for **Structure-B**. To explain the NMR results, an exchange mechanism between these two types of basic solvation structures in the mixture electrolytes containing both $Mg(BH_4)_2$ and $Mg(TFSI)_2$ in DGM is suggested. For 0.01 M $Mg(BH_4)_2$ and varied concentration (0.001–0.004 M) of $Mg(TFSI)_2$ in DGM, possible mechanisms include solvent molecular rearrangement and direct Mg-ion exchange between these two structures. It was found that solvent exchange was much faster than the direct Mg-ion exchange due to the lower energy required. For the solvent exchange mechanism, an intermediate **Structure-C** with its first solvation shell similar to **Structure-A,** but with one BH_4 replaced by a TFSI anion is likely responsible for facilitating the process. **Structure-C** is also the dominant solvation structure in the mixture containing both $Mg(BH_4)_2$ and $Mg(TFSI)_2$ at high salt concentrations (0.1 M or higher for each salt) in DGM. The exchange between **Structure-C** and **Structure-B** explains the observed ^{25}Mg chemical shifts at high salt concentrations. Finally, cyclic voltammetry and coulombic efficiency measurements of the different electrolyte compositions indicate that the efficiency of reversible plating/stripping of Mg strongly depends on the concentration and the ratios of $Mg(BH_4)_2$ and $Mg(TFSI)_2$ in DGM, and the efficiency is optimized at a $Mg(BH_4)_2$ to $Mg(TFSI)_2$ ratio of approximately 1:4 due to both enhanced dynamics in solution and improved stability the TFSI anion.

Acknowledgments

This work was supported by the Joint Center for Energy Storage Research (JCESR), an Energy Innovation Hub funded by the U.S. Department of Energy, Office of Science, Office of Basic Energy Sciences (BES). The NMR and first principle computational studies were conducted in the William R. Wiley Environmental Molecular Sciences Laboratory (EMSL), a national scientific user facility sponsored by DOE's Office of Biological and Environmental Research (BER) and located at PNNL. The classical molecular dynamics simulations were performed using the computational resources of the National Energy Research Scientific Computing Center (NERSC), which is supported by the Office of Science of the U.S. Department of Energy under Contract No. DE-AC02-05CH11231. PNNL is operated by Battelle for the Department of Energy under Contract DE-AC05-76RL01830.

Appendix A. Supplementary material

Supplementary data associated with this article can be found in the online version at http://dx.doi.org/10.1016/j.nanoen.2018.01.051.

References

[1] Y.Y. Shao, et al., Coordination chemistry in magnesium battery electrolytes: how ligands affect their performance, Sci. Rep. (2013) 3.
[2] J. Muldoon, et al., Electrolyte roadblocks to a magnesium rechargeable battery, Energy Environ. Sci. 5 (3) (2012) 5941–5950.
[3] N. Pour, et al., Structural analysis of electrolyte solutions for rechargeable Mg batteries by stereoscopic means and DFT calculations, J. Am. Chem. Soc. 133 (16) (2011) 6270–6278.
[4] H.S. Kim, et al., Structure and compatibility of a magnesium electrolyte with a sulphur cathode, Nat. Commun. (2011) 2.
[5] Z. Cao, Y. Peng, G.A. Voth, Ion transport through ultrathin electrolyte under applied voltages, J. Phys. Chem. B 119 (24) (2015) 7516–7521.
[6] X.Y. Li, J. Nie, Density functional theory study on metal bis(trifluoromethylsulfonyl)imides: electronic structures, energies, catalysis, and predictions, J. Phys. Chem. A 107 (31) (2003) 6007–6013.
[7] J. Muldoon, et al., Corrosion of magnesium electrolytes: chlorides – the culprit, Energy Environ. Sci. 6 (2) (2013) 482–487.
[8] C. Liang, K. Kwak, M. Cho, Revealing the solvation structure and dynamics of carbonate electrolytes in lithium-ion batteries by two-dimensional infrared spectrum modeling, J. Phys. Chem. Lett. 8 (23) (2017) 5779–5784.
[9] L. Suo, et al., "Water-in-salt" electrolyte enables high-voltage aqueous lithium-ion chemistries, Science 350 (6263) (2015) 938–943.
[10] T. Watkins, D.A. Buttry, Determination of Mg2+ Speciation in a TFSI–based ionic liquid with and without chelating ethers using raman spectroscopy, J. Phys. Chem. B 119 (23) (2015) 7003–7014.
[11] M. Salama, et al., Unique behavior of dimethoxyethane (DME)/Mg (N (SO2CF3) 2) 2 solutions, J. Phys. Chem. C. (2016).
[12] A. Baskin, D. Prendergast, Exploration of the detailed conditions for reductive stability of $Mg(TFSI)_2$ in diglyme: implications for multivalent electrolytes, J. Phys. Chem. C 120 (7) (2016) 3583–3594.
[13] T. Watkins, A. Kumar, D.A. Buttry, Designer ionic liquids for reversible electrochemical deposition/dissolution of magnesium, J. Am. Chem. Soc. 138 (2) (2016) 641–650.
[14] S.S. Zhang, Liquid electrolyte lithium/sulfur battery: fundamental chemistry, problems, and solutions, J. Power Sources 231 (2013) 153–162.
[15] P. Wang, et al., Mixed ionic liquids as electrolyte for reversible deposition and dissolution of magnesium, Surf. Coat. Technol. 201 (6) (2006) 3783–3787.
[16] S.F. Amalraj, D. Aurbach, The use of in situ techniques in R&D of Li and Mg rechargeable batteries, J. Solid State Electrochem. 15 (5) (2011) 877–890.
[17] H.S. Kim, et al., Structure and compatibility of a magnesium electrolyte with a sulphur cathode, Nat. Commun. 2 (2011) 427.
[18] D. Aurbach, et al., Prototype systems for rechargeable magnesium batteries, Nature 407 (6805) (2000) 724–727.
[19] D. Aurbach, et al., Progress in rechargeable magnesium battery technology, Adv. Mater. 19 (23) (2007) 4260–4267.
[20] O. Mizrahi, et al., Electrolyte solutions with a wide electrochemical window for recharge magnesium batteries, J. Electrochem. Soc. 155 (2) (2008) A103–A109.
[21] Y.S. Guo, et al., Boron-based electrolyte solutions with wide electrochemical windows for rechargeable magnesium batteries, Energy Environ. Sci. 5 (10) (2012) 9100–9106.
[22] A. Ponrouch, et al., Towards a calcium-based rechargeable battery, Nat. Mater. 15 (2) (2016) 169–172.
[23] K.W. Nam, et al., The high performance of crystal water containing manganese birnessite cathodes for magnesium batteries, Nano Lett. 15 (6) (2015) 4071–4079.
[24] E. Levi, Y. Gofer, D. Aurbach, On the way to rechargeable mg batteries: the challenge of new cathode materials, Chem. Mater. 22 (3) (2010) 860–868.
[25] O. Mizrahi, et al., Electrolyte solutions with a wide electrochemical window for rechargeable magnesium batteries, J. Electrochem. Soc. 155 (2) (2008) A103.
[26] Y. Gofer, et al., Improved electrolyte solutions for rechargeable magnesium batteries, Electrochem. Solid-State Lett. 9 (5) (2006) A257.
[27] C.B. Bucur, et al., Confession of a magnesium battery, J. Phys. Chem. Lett. 6 (18) (2015) 3578–3591.
[28] J. Muldoon, C.B. Bucur, T. Gregory, Quest for nonaqueous multivalent secondary batteries: magnesium and beyond, Chem. Rev. 114 (23) (2014) 11683–11720.
[29] P. Saha, et al., Rechargeable magnesium battery: current status and key challenges for the future, Progress. Mater. Sci. (2014).
[30] Z. Lu, et al., On the electrochemical behavior of magnesium electrodes in polar aprotic electrolyte solutions, J. Electroanal. Chem. 466 (2) (1999) 203–217.
[31] D. Aurbach, et al., A comparison between the electrochemical behavior of reversible magnesium and lithium electrodes, J. Power Sources 97–8 (2001) 269–273.
[32] D. Aurbach, et al., Nonaqueous magnesium electrochemistry and its application in secondary batteries, Chem. Rec. 3 (1) (2003) 61–73.
[33] N. Amir, et al., Progress in nonaqueous magnesium electrochemistry, J. Power Sources 174 (2) (2007) 1234–1240.
[34] H.D. Yoo, et al., Mg rechargeable batteries: an on-going challenge, Energy Environ. Sci. 6 (8) (2013) 2265–2279.
[35] J. Muldoon, C.B. Bucur, T. Gregory, Fervent hype behind magnesium batteries: an open call to synthetic chemists-electrolytes and cathodes needed, Angew. Chem. (2017).
[36] I. Shterenberg, et al., The challenge of developing rechargeable magnesium batteries, MRS Bull. 39 (05) (2014) 453–460.
[37] H.S. Kim, et al., Structure and compatibility of a magnesium electrolyte with a sulphur cathode, Nat. Commun. 2 (2011) 427.
[38] R. Mohtadi, et al., magnesium borohydride: from hydrogen storage to magnesium battery, Angew. Chem.-Int. Ed. 51 (39) (2012) 9780–9783.
[39] S.H. Lapidus, et al., Solvation structure and energetics of electrolytes for multivalent energy storage (PCCP), Phys. Chem. Chem. Phys. 16 (40) (2014) 21941–21945.
[40] S.-Y. Ha, et al., magnesium(II) Bis(trifluoromethane sulfonyl) imide-based electrolytes with wide electrochemical windows for rechargeable magnesium batteries, ACS Appl. Mater. Interfaces 6 (6) (2014) 4063–4073.
[41] N.N. Rajput, et al., The coupling between stability and ion pair formation in magnesium electrolytes from first-principles quantum mechanics and classical molecular dynamics, J. Am. Chem. Soc. 137 (9) (2015) 3411–3420.
[42] Y. Shao, et al., Coordination chemistry in magnesium battery electrolytes: how ligands affect their performance, Sci. Rep. (2013) 3.
[43] N. Sa, et al., Role of chloride for a simple, non-grignard Mg electrolyte in ether-based solvents, ACS Appl. Mater. Interfaces 8 (25) (2016) 16002–16008.
[44] I. Shterenberg, et al., Evaluation of (CF3SO2)2N − (TFSI) based electrolyte solutions for Mg batteries, J. Electrochem. Soc. 162 (13) (2015) A7118–A7128.
[45] Y. Cheng, et al., Electrochemically stable cathode current collectors for rechargeable magnesium batteries, J. Mater. Chem. A 2 (8) (2014) 2473–2477.
[46] M.Y. Hu, et al., In situ natural abundance ^{17}O and ^{25}Mg NMR investigation of aqueous $Mg(OH)_2$ dissolution in the presence of supercritical CO_2, Environ. Sci. Technol. 50 (22) (2016) 12373–12384.
[47] C. Wan, et al., Natural abundance ^{17}O, ^{6}Li NMR and molecular modeling studies of the solvation structures of lithium bis(fluorosulfonyl)imide/1,2-dimethoxyethane liquid electrolytes, J. Power Sources 307 (2016) 231–243.
[48] X. Deng, et al., Natural abundance ^{17}O nuclear magnetic resonance and computational modeling studies of lithium based liquid electrolytes, J. Power Sources 285 (2015) 146–155.
[49] Baerends, E.J.A., J, J.A. Berger, A. Be´rces, F.M. Bickelhaupt, C. Bo, P.L. de Boeij, P. M. Boerrigter, L. Cavallo, D.P. Chong, L. Deng, R.M. Dickson, D.E. Ellis, M. van Faassen, L. Fan, T.H. Fischer, C. Fonseca Guerra, S.J.A. van Gisbergen, A.W. Go¨ tz, J.A. Groeneveld, O.V. Gritsenko, M. Gru¨ ning, F.E. Harris, P. van den Hoek, C.R. Jacob, H. Jacobsen, L. Jensen, E.S. Kadantsev, G. van Kessel, R. Klooster, F. Kootstra, M.V. Krykunov, E. van Lenthe, J.N. Louwen, D.A. McCormack, A. Michalak, J. Neugebauer, V.P. Nicu, V.P. Osinga, S. Patchkovskii, P.H.T. Philipsen, D. Post, C.C. Pye, W. Ravenek, J.I. Rodriguez, P. Romaniello, P. Ros, P.R.T. Schipper, G. Schreckenbach, J.G. Snijders, M. Sola´, M. Swart, D. Swerhone, G. te Velde, P. Vernooijs, L. Versluis, L. Visscher, O. Visser, F. Wang, T.A. Wesolowski, E. M. van Wezenbeek, G. Wiesenekker, S.K. Wolff, T.K. Woo, A.L. Yakovlev, T. Ziegler, Amsterdam Density Functional. Theoretical Chemistry, Scientific Computing & Modelling (SCM), Theoretical Chemistry, Vrije Universiteit: Amsterdam, The Netherlands. (URL: ⟨http://www.scm.com⟩).
[50] A.D. Becke, Density-functional exchange-energy approximation with correct asymptotic behavior, Phys. Rev. A 38 (6) (1988) 3098–3100.
[51] C.T. Lee, W.T. Yang, R.G. Parr, Development of the colle-salvetti correlation-energy formula into a functional of the electron-density, Phys. Rev. B. 37 (2) (1988) 785–789.
[52] S. Grimme, et al., Density functional theory with dispersion corrections for supramolecular structures, aggregates, and complexes of (bio)organic molecules, Org. Biomol. Chem. 5 (5) (2007) 741–758.
[53] E. Van Lenthe, E.J. Baerends, Optimized slater-type basis sets for the elements 1-118, J. Comput. Chem. 24 (9) (2003) 1142–1156.
[54] S. Pronk, et al., GROMACS 4.5: a high-throughput and highly parallel open source molecular simulation toolkit, Bioinformatics (2013) btt055.
[55] Y. Shao, et al., Nanocomposite polymer electrolyte for rechargeable magnesium batteries, Nano Energy 12 (2015) 750–759.
[56] J. Wang, et al., Development and testing of a general amber force field, J. Comput. Chem. 25 (9) (2004) 1157–1174.
[57] J. Wang, et al., Automatic atom type and bond type perception in molecular mechanical calculations, J. Mol. Graph. Model. 25 (2) (2006) 247–260.

[58] C.I. Bayly, et al., A well-behaved electrostatic potential based method using charge restraints for deriving atomic charges: the RESP model, J. Phys. Chem. 97 (40) (1993) 10269–10280.
[59] H.J. Berendsen, et al., Molecular dynamics with coupling to an external bath, J. Chem. Phys. 81 (8) (1984) 3684–3690.
[60] R. Mohtadi, et al., magnesium borohydride: from hydrogen storage to magnesium battery, Angew. Chem. Int. Ed. 51 (39) (2012) 9780–9783.
[61] N.N. Rajput, et al., The coupling between stability and ion pair formation in magnesium electrolytes from first-principles quantum mechanics and classical molecular dynamics, J. Am. Chem. Soc. 137 (2015) 3411–3420.
[62] N. Sa, et al., Concentration dependent electrochemical properties and structural analysis of a simple magnesium electrolyte: magnesium bis (trifluoromethane sulfonyl) imide in diglyme, RSC Adv. 6 (114) (2016) 113663–113670.
[63] O. Borodin, G.D. Smith, LiTFSI structure and transport in ethylene carbonate from molecular dynamics simulations, J. Phys. Chem. B 110 (10) (2006) 4971–4977.

Jian Zhi Hu obtained his Ph.D. in Applied Physics in 1994 from a Joint-Training Pro-gram between Wuhan Institute of Physics, the Chinese Academy of Sciences and the Department of Chemistry, University of Utah, USA. He did his postdoctoral studies also from University of Utah. Currently, he is a senior staff scientist of Pacific Norwest National Laboratory, specialized in nuclear magnetic resonance (NMR) spectroscopy and imaging. He has published more than 190 peer reviewed papers related to NMR. He received 10 US patents and two R&D 100 awards.

Nav Nidhi Rajput obtained her Ph.D. in Chemical Engineering at Louisiana State University in Louisiana, USA in 2013. She joined LBNL as a Postdoctoral Fellow at environmental energy technology division in 2013. Her research interests include molecular dynamics simulations to acceler-ate discovery of novel electrolytes for bat-teries and supercapacitors.

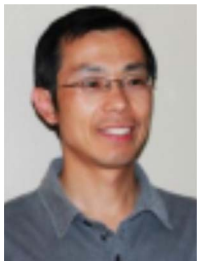

Yuyan Shao received his Ph.D. from Harbin Institute of Technology. He is a Senior Scientist in the Energy Processes and Mate-rials Division of the Pacific Northwest National Laboratory. His research is focused on the fundamental study and high-performance functional materials for electrochemical energy conversion and storage, including fuel cells, batteries, supercapaci-tors, etc. He is named in Thomson Reuters' Highly Cited Researchers-2014. He has published over 80 papers.

Nicholas Jaegers obtained his B.S. in Chemical Engineering from Iowa State University in 2014. He is a Ph.D. candidate in Chemical Engineering at Washington State University within Dr. Yong Wang's research group. He is currently located at Pacific Northwest National Laboratory as an intern focusing on applications of nuclear magnetic resonance in catalysis.

Karl Mueller received his Ph.D. from the University of California, Berkeley and is the Chief Science and Technology Officer for Physical and Computational Sciences at Pacific Northwest national Laboratory. His research focuses on the use of NMR methods to address structural and dynamic questions in complex systems, including batteries and catalyst materials. He is a AAAS Fellow and has published over 140 papers.

Jun Liu received his Ph.D. in materials science from University of Washington. He is a Laboratory Fellow and Energy Processes and Materials Division Director at the Pacific Northwest National Laboratory. Dr. Liu's main research interest includes synthesis of functional nanomaterials for energy sto-rage, catalysis, environmental separation and health care. He has received more than 40 U.S. patents, two R&D 100 Awards, two BES Awards for Significant Impact on DOE Missions, and was named 2007 Distinguished Inventor of Battelle. Dr. Liu is an AAAS Fellow and MRS Fellow. He is named in Thomson Reuters' Highly Cited Researchers-2014 in three categories (Materials science, Chemistry and Engineering). He has over 300 publications.

Kristin Aslaug Persson obtained her Ph.D. in Theoretical Physics at the Royal Institute of Technology in Stockholm, Sweden in 2001. She is an Associate Professor in Materials Science and Engineering at UC Berkeley with a joint appointment as Faculty Staff Scientist at LBNL where she leads The Materials Project (www.materialsproject.org) and the Cross-Cutting thrust in the Joint Center for Energy Storage Research (JCESR) (www.jcesr.org). In 2009 she co-founded the clean-energy start-up Pellion Technologies Inc. (www.pelliontech.com), recipient of an ARPA-E award in 2010 for developing high-energy rechargeable magnesium batteries.